SAND2019-12407C

Time Evolution of Atmospheric Pitting Damage on 304 Stainless Steel

J. Srinivasan[1], T. D. Weirich[1], G. A. Marino[1], A. R. Annerino[1], J. M. Taylor[2], M. A. Melia[2], R. F. Schaller[2], C. R. Bryan[2], G. S. Frankel[1], J. S. Locke[1], E. J. Schindelholz[2]

[1]Fontana Corrosion Center, Department of Materials Science and Engineering, The Ohio State University
[2]Sandia National Laboratories*

Sandia National Laboratories is a multi-mission laboratory managed and operated by National Technology and Engineering Solutions of Sandia, LLC., a wholly owned subsidiary of Honeywell International, Inc., for the U.S. Department of Energy's National Nuclear Security Administration under contract DE-NA0003525.

Max pit size predictive analyses have modeled limiting pit depth in long-time exposures

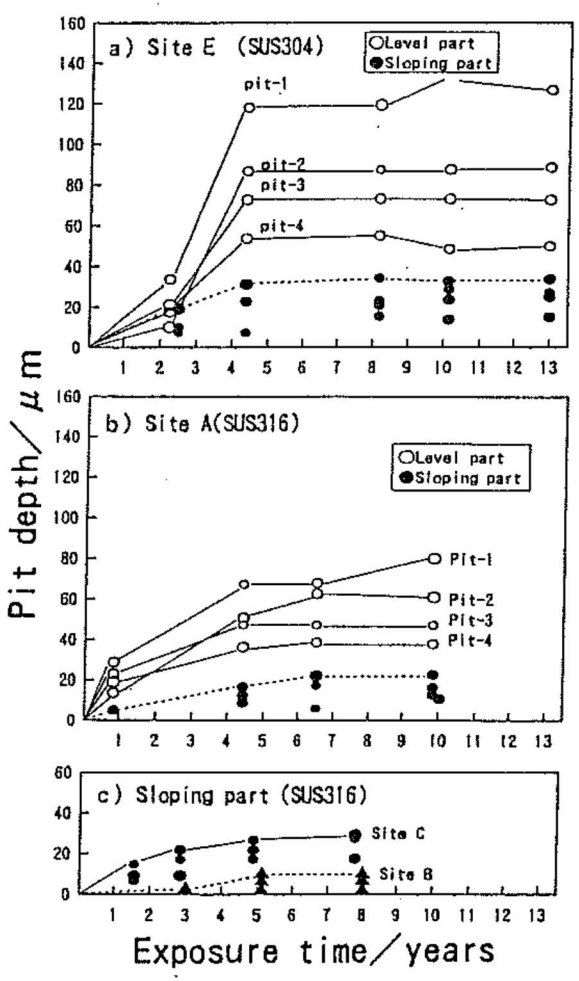

M. Nakata, N. Ono, Y. Usada, *Corrosion Engineering,* 46, 655-666 (1997)

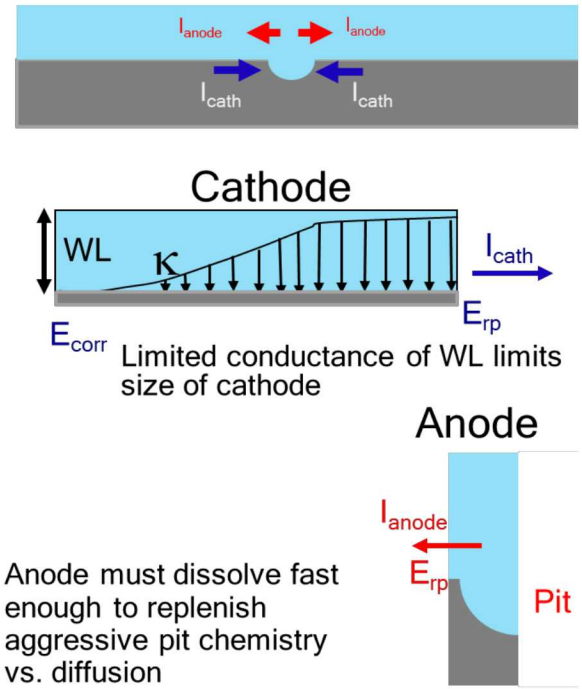

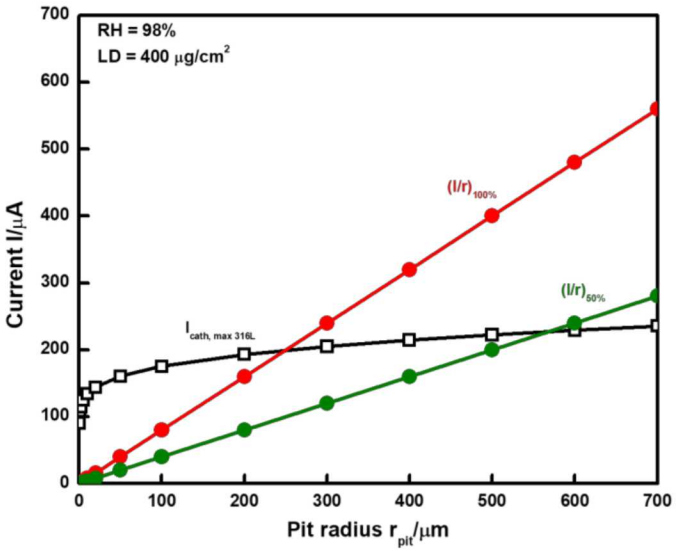

Max pit size assumes hemispherical pit, thin film electrolyte

Nanoscale salt aerosols deposit on sheltered storage sites, form corrosive brine → pitting risk

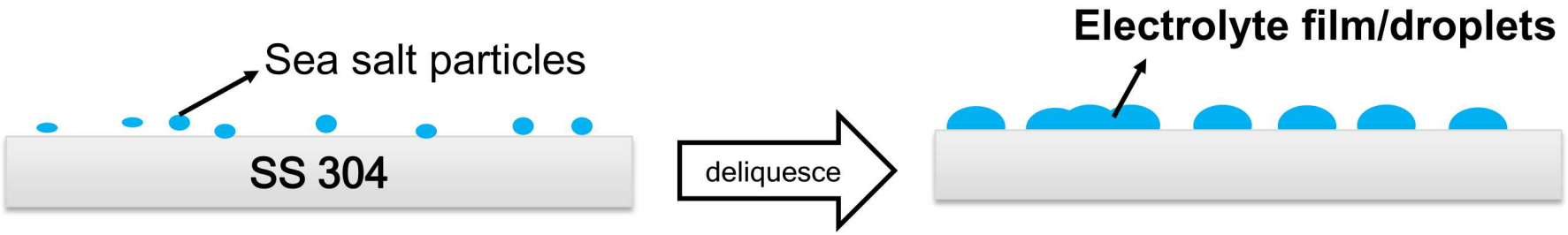

RH	$[Cl^-]$ $(mol \cdot kg^{-1})$	$[Na^+]$ $(mol \cdot kg^{-1})$	$[Mg^{2+}]$ $(mol \cdot kg^{-1})$
40%	10.45	0.18	5.33
76%	5.65	4.85	0.54

High chloride concentration in electrolyte leads to pitting risk
RH variation → electrolyte chemistry changes, impacts pitting kinetics

How does atmospheric environment affect pitting and SCC?

Key questions:

- How does RH affect:
  - pit density? corrosion damage? pit morphology?
- What implications do these results have on limiting pit size?
- What features are likely to cause crack initiation?

Approach:

- Print sea salt on coupons, expose for different times to 40% and 76% RH
- Characterize using EBSD, optical profilometry, FIB-SEM
- Rationalize RH effect on pitting kinetics and morphology

Near-surface local deformation from grinding results in cross-hatched pattern of slip bands

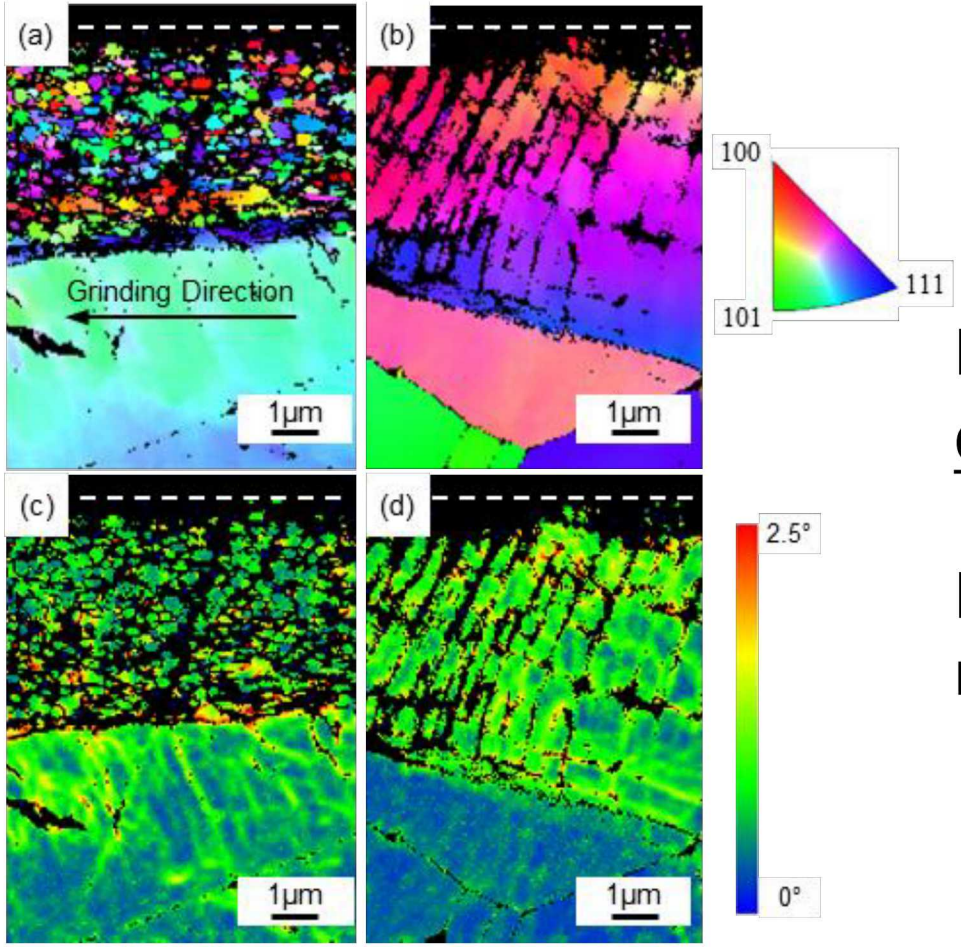

Deformation slip bands form <u>cross-hatch pattern</u>

Non-indexable near-surface nanocrystalline layer

Weirich et al. JECS (2019).

Pit distribution uniform, localized to droplet at low RH
Droplet spreading, pit clustering at high RH

40%RH **76%RH**

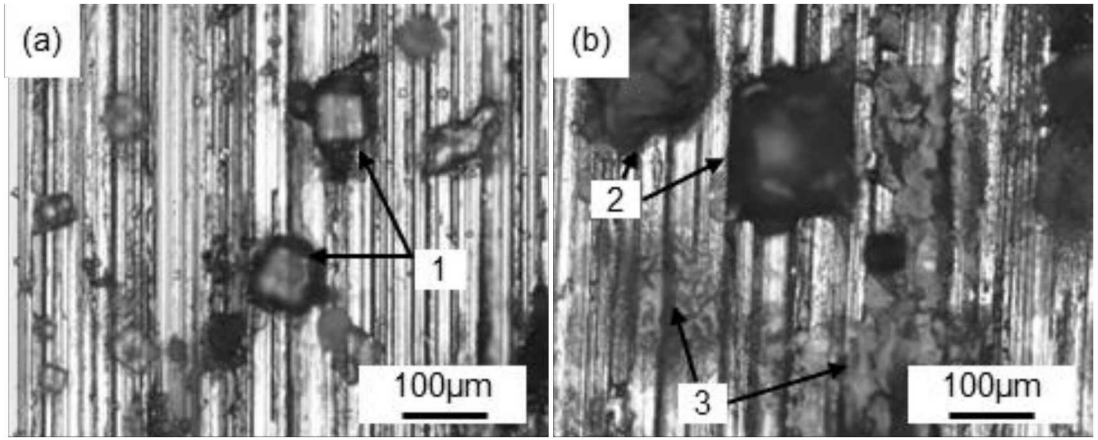

Minimal spreading

Translucent films, salt redistribution

40%RH **76%RH**

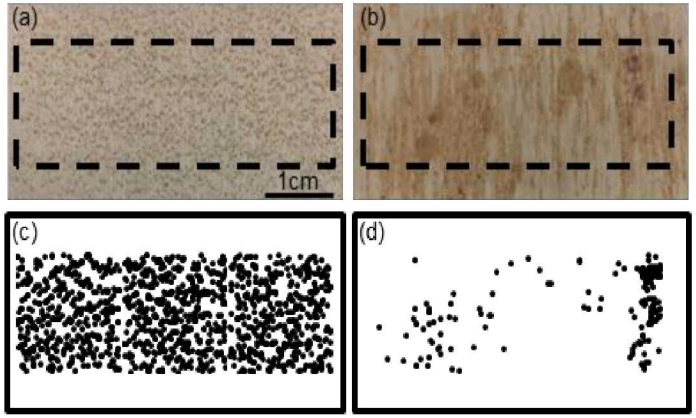

Uniform pit distribution

Pit clustering

Salt loading density = 300 μg/cm^2
T = 35 ˚C
Ground surface
t = 1 year

Number of pits at 40% RH ≈8x at 76% RH

Pit density approaches limiting values at long times

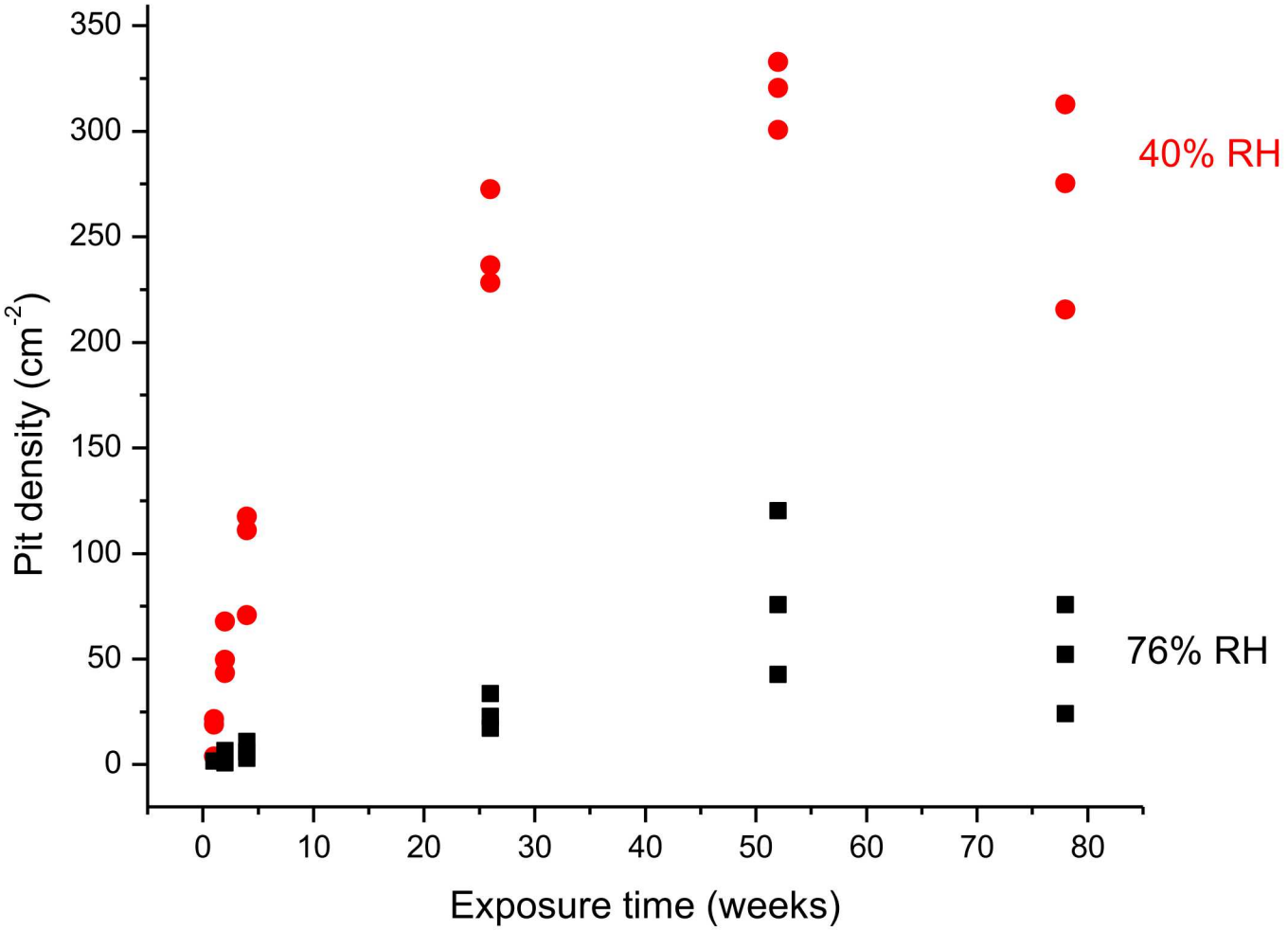

Corrosion damage approaches limiting values at long times

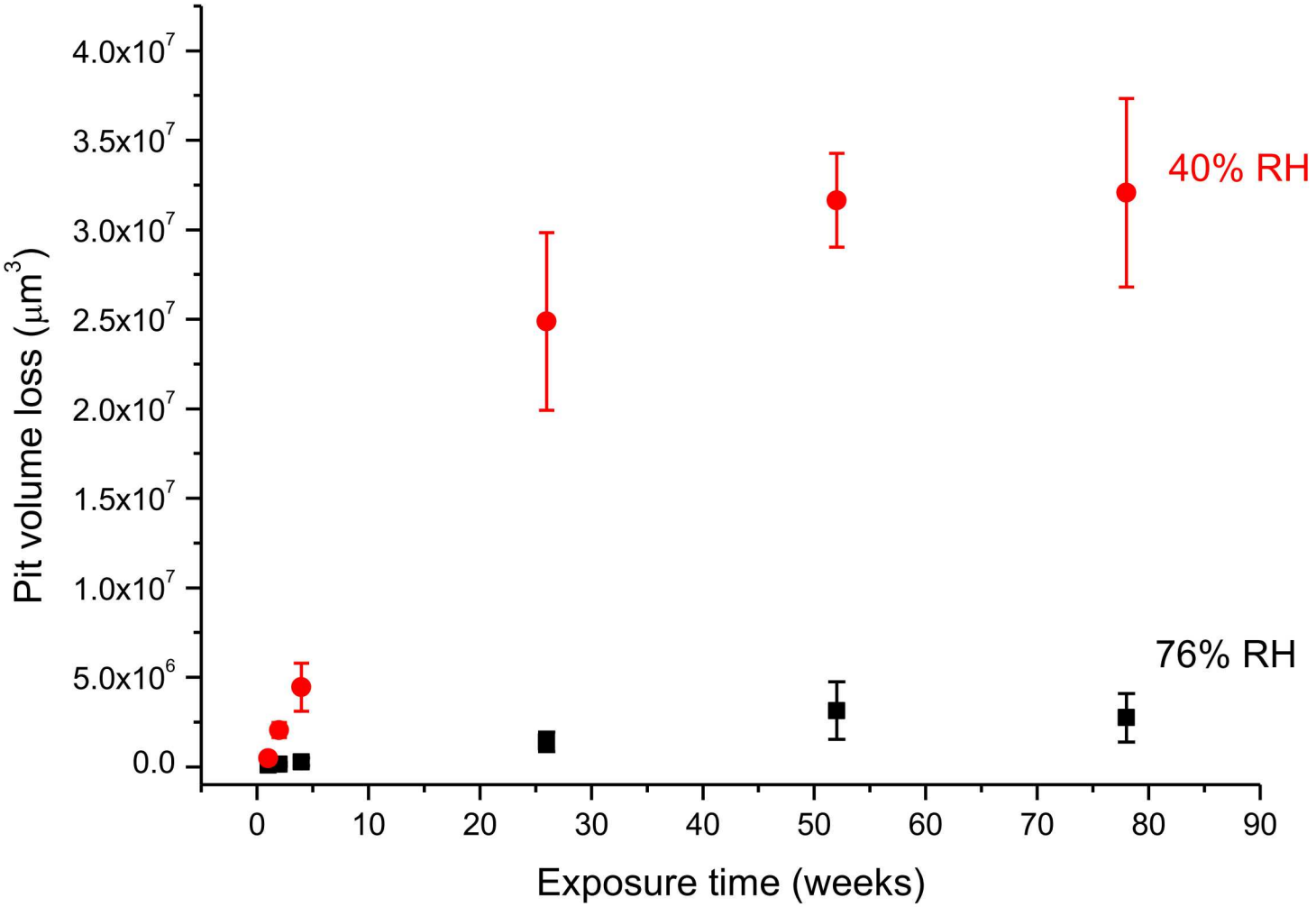

Low RH damage plateaus 52 weeks onwards, high RH 26 weeks onwards

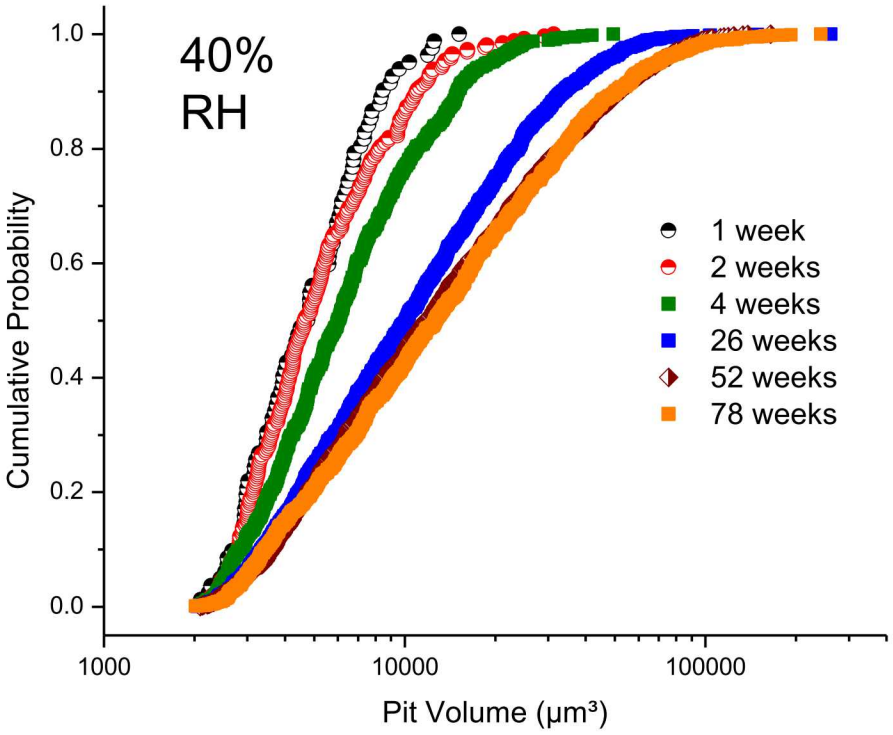

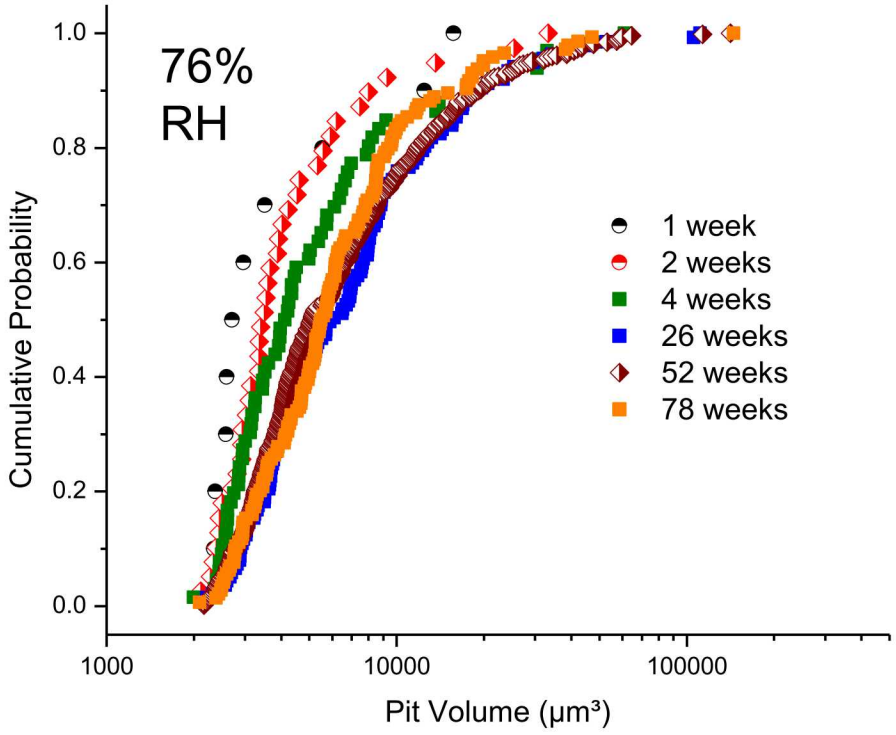

Similarity in probability distributions evaluated by K-S tests at the p=0.05 level

RH distinctly affects pit morphology across all exposure times

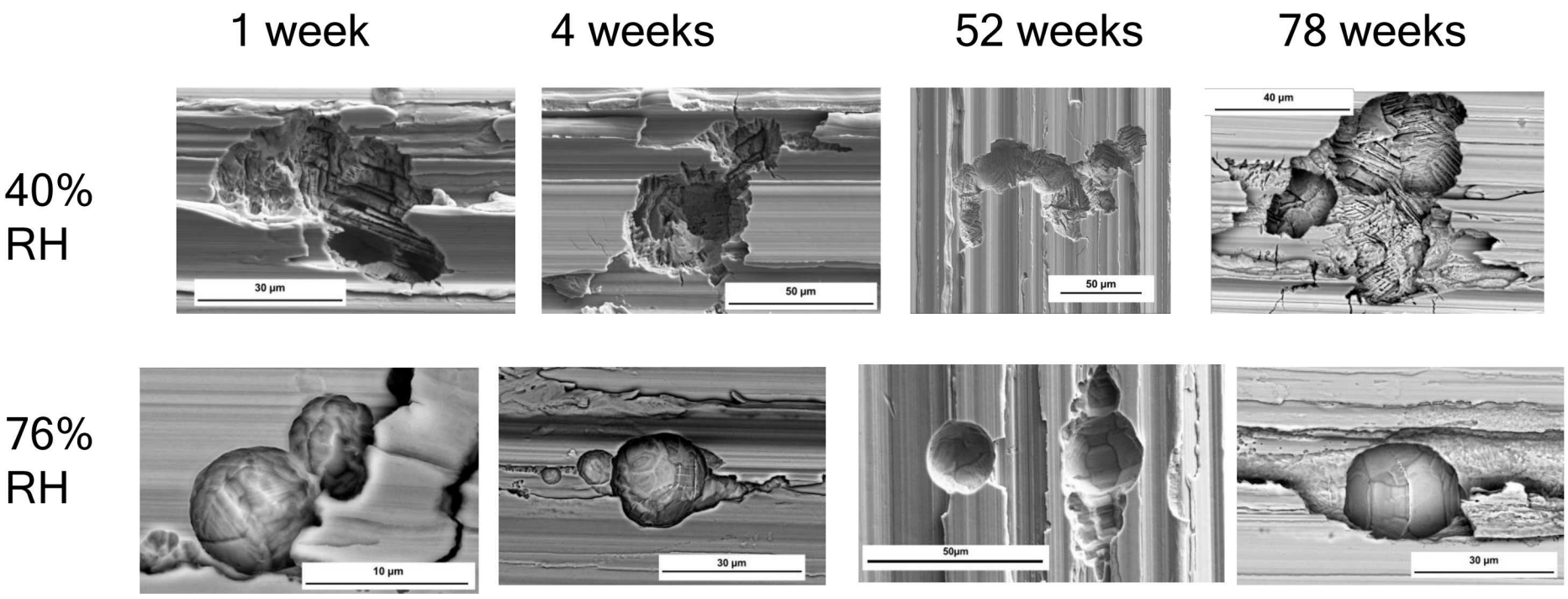

Low RH → **cross-hatched morphology, cracks emanating from pits**

High RH → **faceted ellipsoids**

RH affects physicochemical properties that influence pitting

RH	$[Cl^-]$ $(mol \cdot kg^{-1})$	$[Na^+]$ $(mol \cdot kg^{-1})$	$[Mg^{2+}]$ $(mol \cdot kg^{-1})$	$[O_2]$ $(mol \cdot kg^{-1})$	η (cP)	κ $(mS \cdot cm^{-1})$	ρ $(kg \cdot m^{-3})$	D_{O2} $(m^2 \cdot s^{-1})$	V_{RH} / V_{76}
40%	10.45	0.18	5.33	2.7×10^{-5}	8.31	125	1330	9.7×10^{-11}	.052
76%	5.65	4.85	0.54	5.1×10^{-5}	1.65	273	1200	4.9×10^{-10}	1

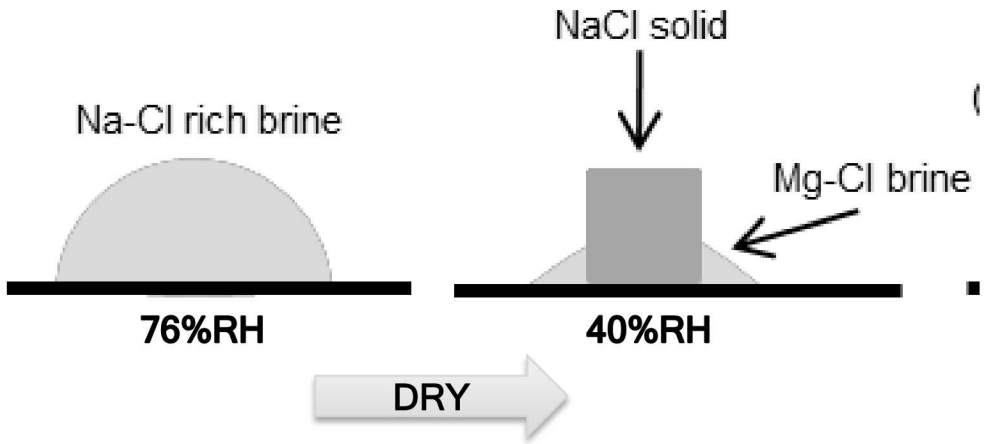

$RH \downarrow = [Cl^-]\uparrow,$
$V \downarrow, \kappa \downarrow, D \downarrow, [O_2]\downarrow$

NaCl precipitates as RH decreases

Discrete droplets at low RH, 2^0 spreading at high RH

RH	$[Cl^-]$ $(mol \cdot kg^{-1})$	$[Na^+]$ $(mol \cdot kg^{-1})$	$[Mg^{2+}]$ $(mol \cdot kg^{-1})$	V_{RH} / V_{76}
40%	10.45	0.18	5.33	.052
76%	5.65	4.85	0.54	1

40%RH

76%RH

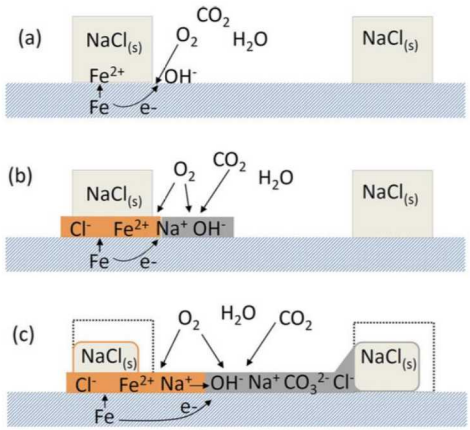

Schindelholz et al. JECS (2014).

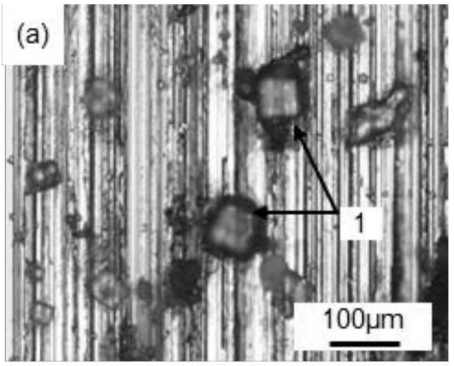

Low RH → low V, high $[Mg^{2+}]$, no spreading

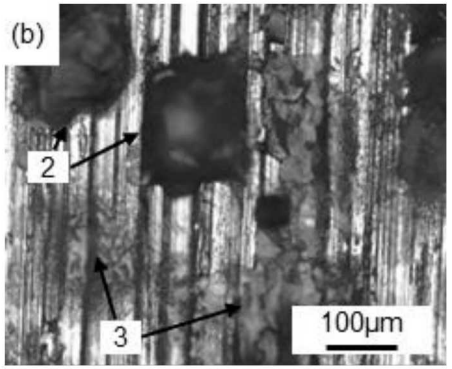

Higher V at high RH → drop coalescence, supported by 2º spreading

Higher [Cl⁻] at low RH facilitates pit initiation

RH	[Cl⁻] (mol·kg⁻¹)
40%	10.45
76%	5.65

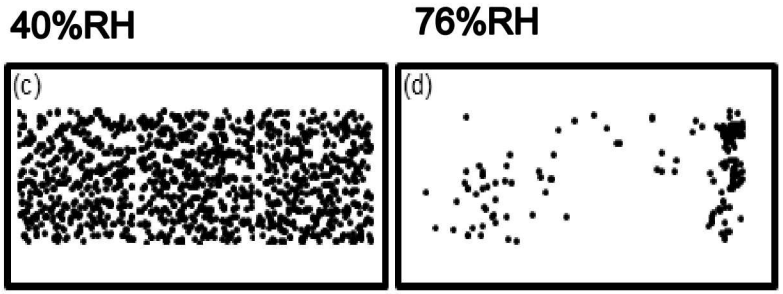

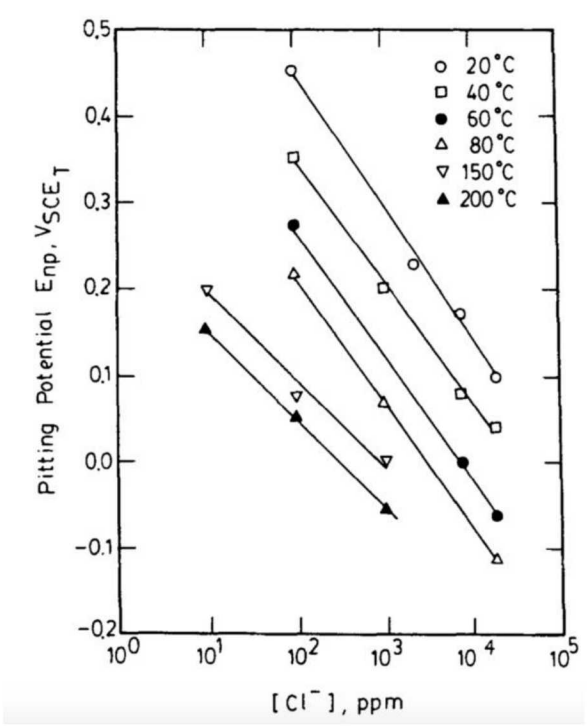

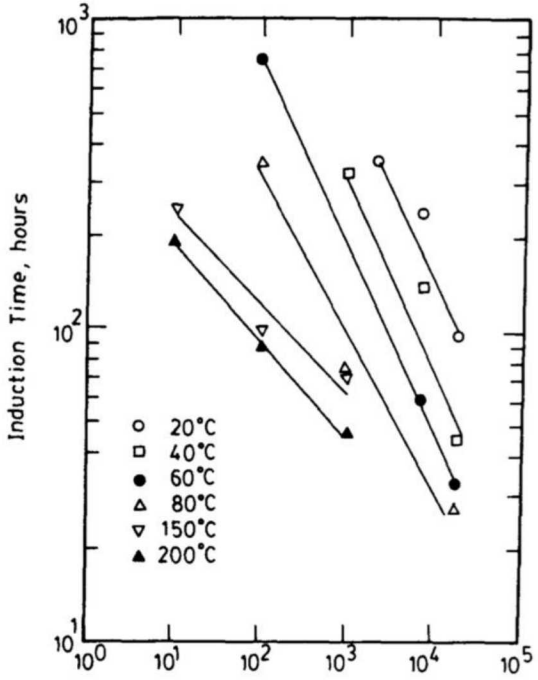

Low RH → High [Cl⁻] multiple pits initiate

High RH → fewer pits initiate due to high E_{pit} required

Wang et al., Corrosion (1988)

Selective attack at low RH resembles deformation slip band pattern

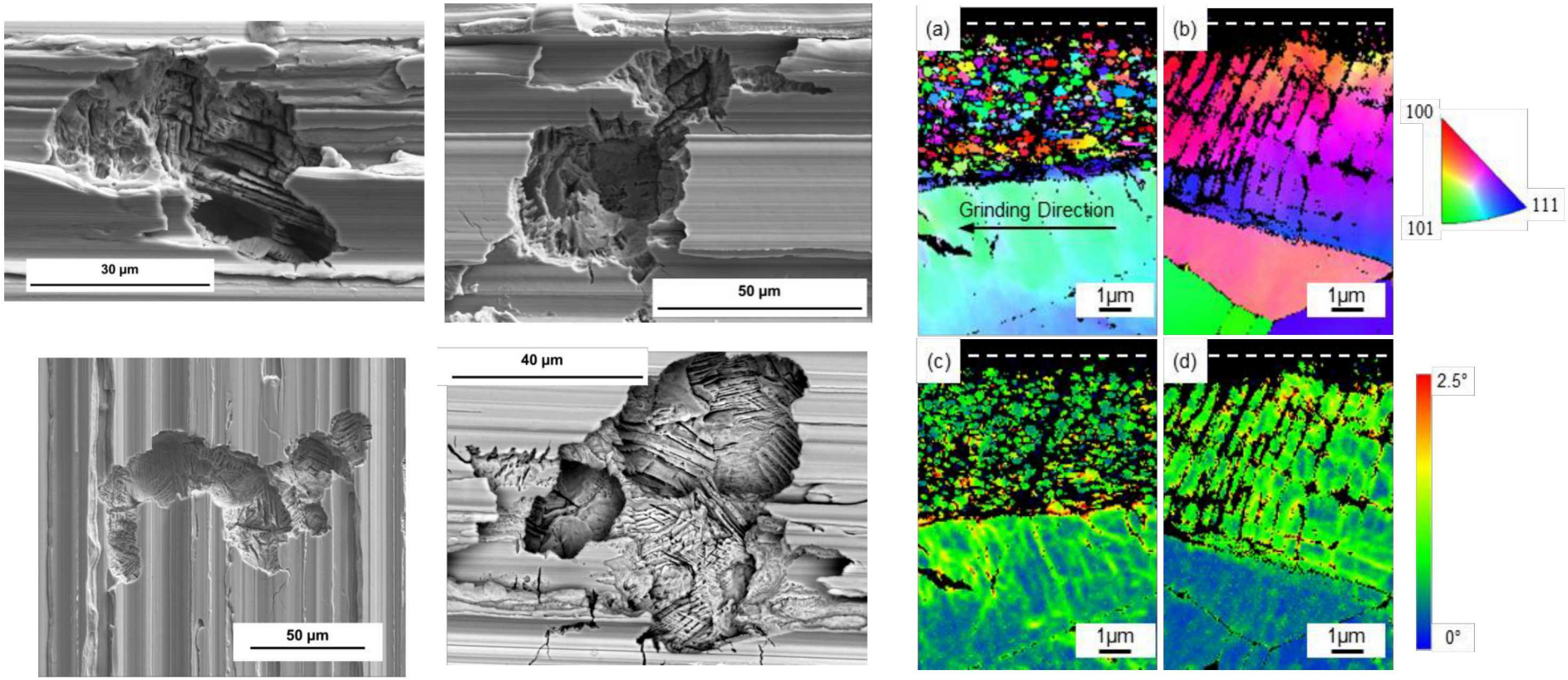

Deformation from grinding may be responsible for morphology at low RH, susceptibility to cracking

Weirich et al. JECS (2019).

Growth near E_{rp} at low RH → cross-hatched morphology
Higher surface concentrations at high RH → faceted ellipsoidal growth

Low RH: Growth close to repassivation limits area for dissolution → fixed active area

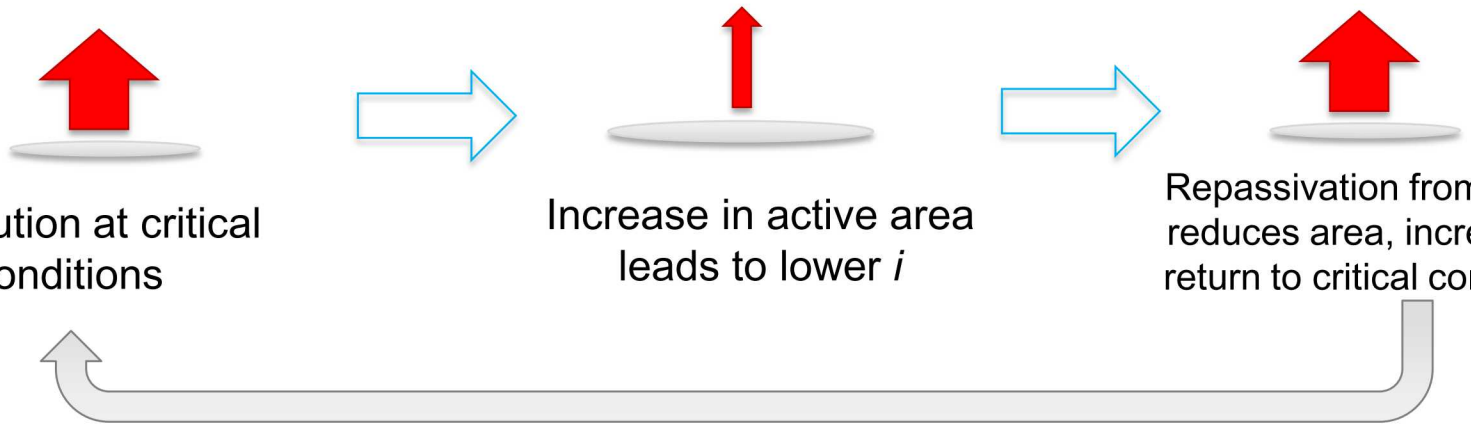

High RH: Growth at potentials between critical stability and saturation with increasing active area

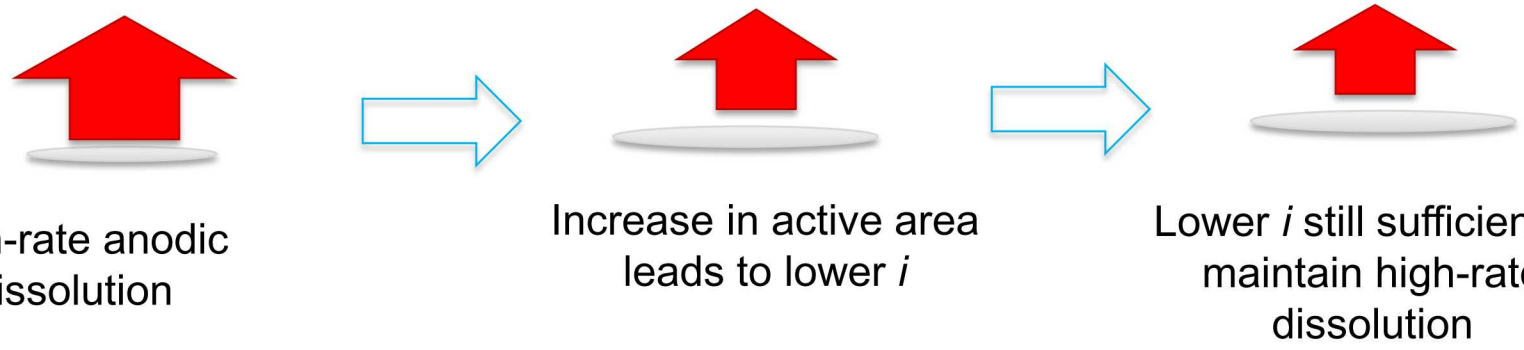

Key takeaway points from current work

- Low RH leads to more corrosion damage, higher pit density
  - No 2^0 spreading, discrete droplets
- Pit density and corrosion damage appear to plateau at long times
- Pit morphology at low RH may be influenced by surface preparation
- Cracks observed near pits at 40% RH exposure
- Pits at high RH smooth, ellipsoidal – high-rate dissolution, low RH growth near E_{rp} – selective attack

Currently open questions and future work

- FIB and/or microCT analysis of larger pits to determine:
  - Are pit shape characteristics well-described by optical profilometry when highly fissured?
  - How deep does micro-pitting penetrate into the surface?
- Hemisphericity assessment of pits and comparison to maximum pit size model
- SCC testing to observe crack initiation from pits based on RH-dependent morphology

SUPPLEMENTAL

User 1

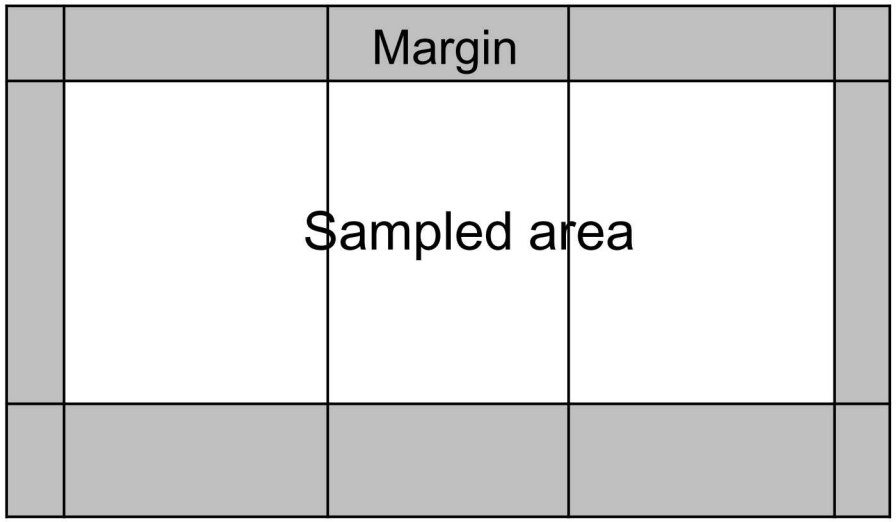

3 equally-spaced areas 12 mm × 12 mm sampled, margin of at least 5 mm away from the edge

User 2

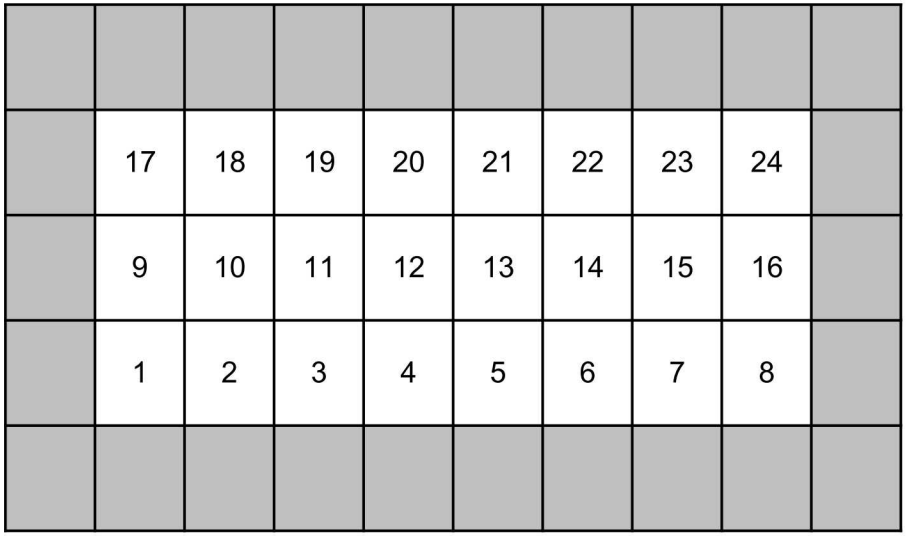

24 equally-spaced area of 5 mm × 5 mm sampled, labeled 1-24, margin of 5 mm from the edge

Fissures/cracks observed only in 40% RH exposures

Images from 52 week exposures

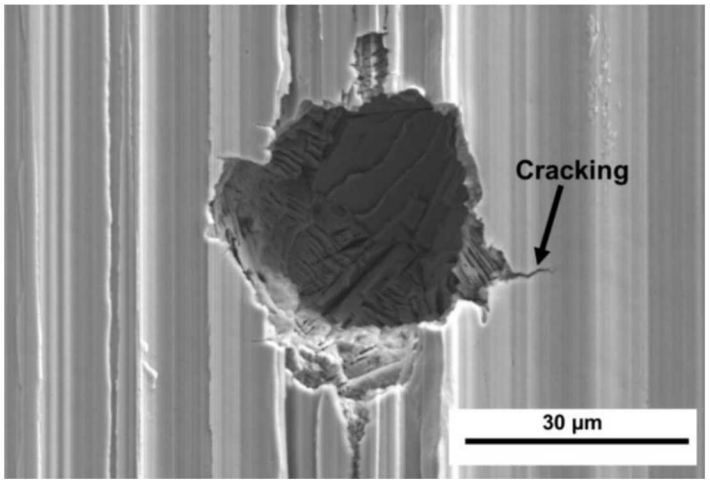

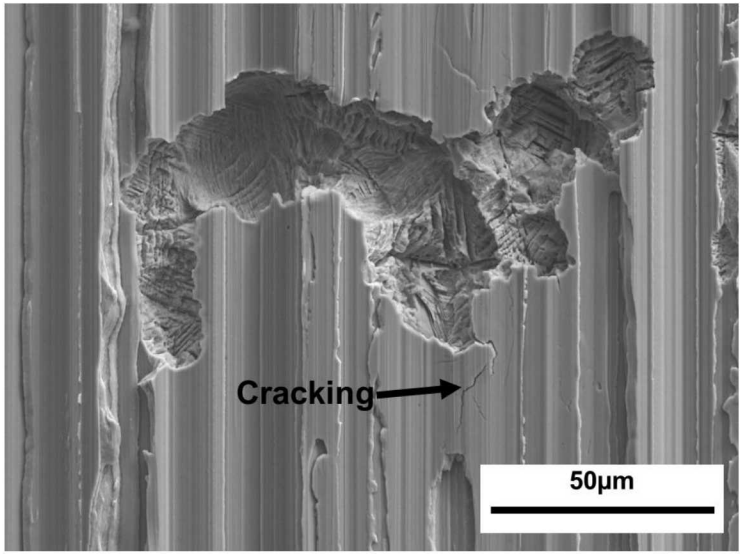

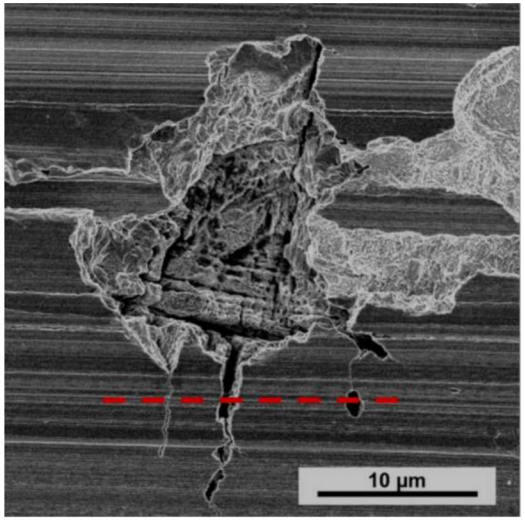

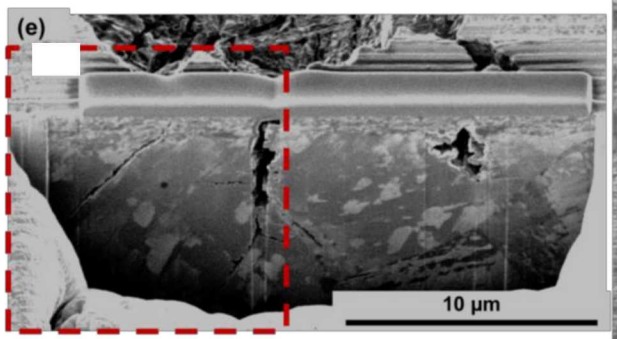

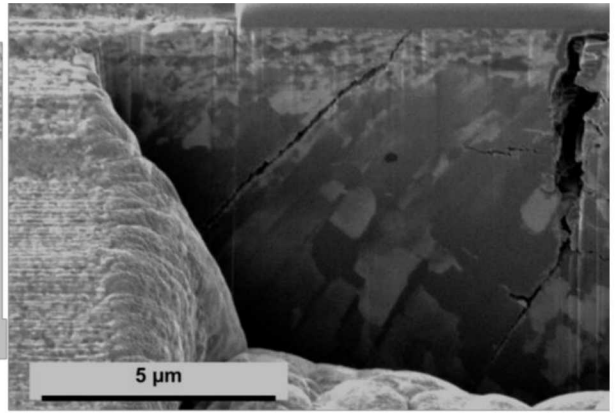

Weirich et al. JECS (2019).

Deformation substructure may contribute to susceptible morphology

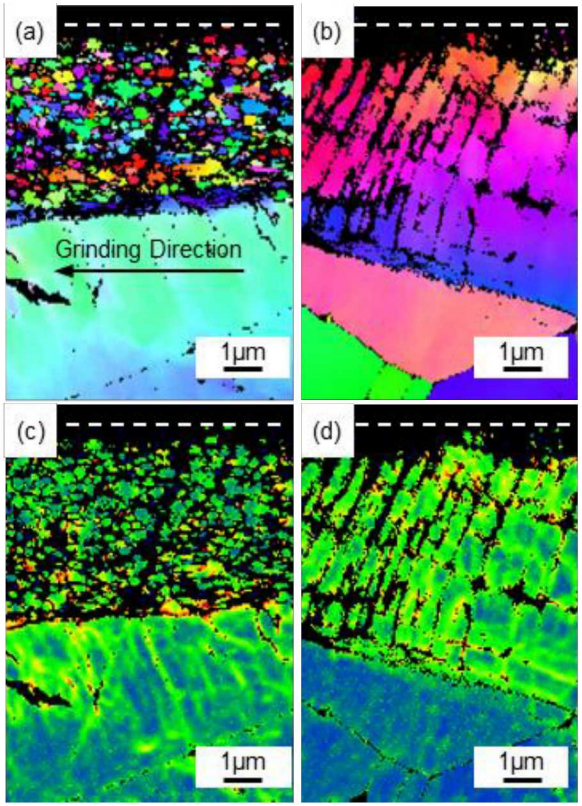

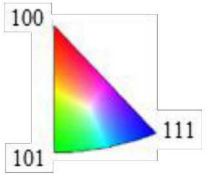

Deformation from grinding may create susceptible microstructure

FIB-SEM of small pits show long cracks

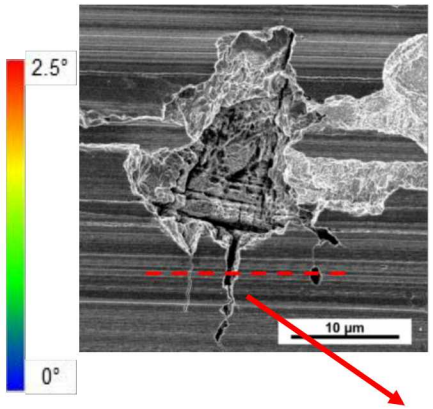

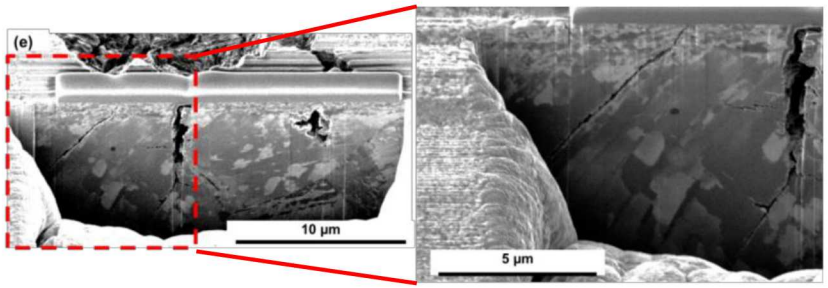

SCC initiator?

Weirich et al. JECS (2019).

Susceptible morphology does not match ferrite distribution

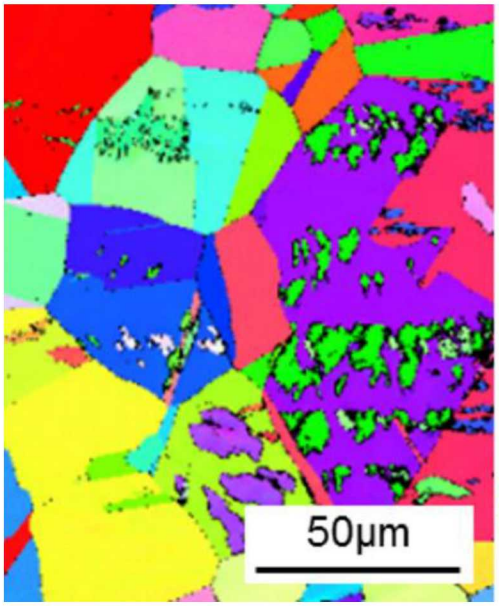

Grain structure map

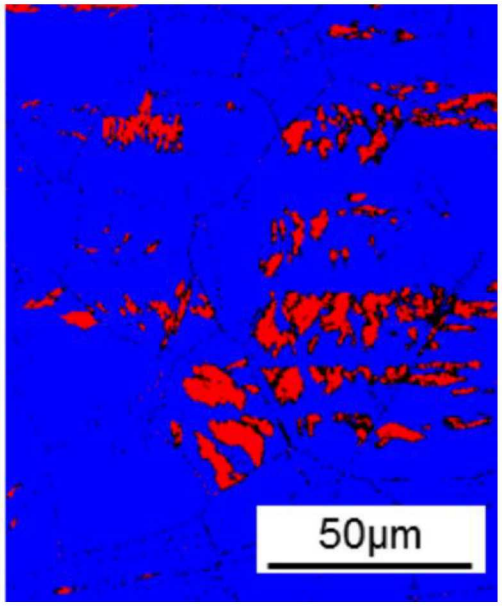

Phase distribution map – red indicates ferrite/martensite

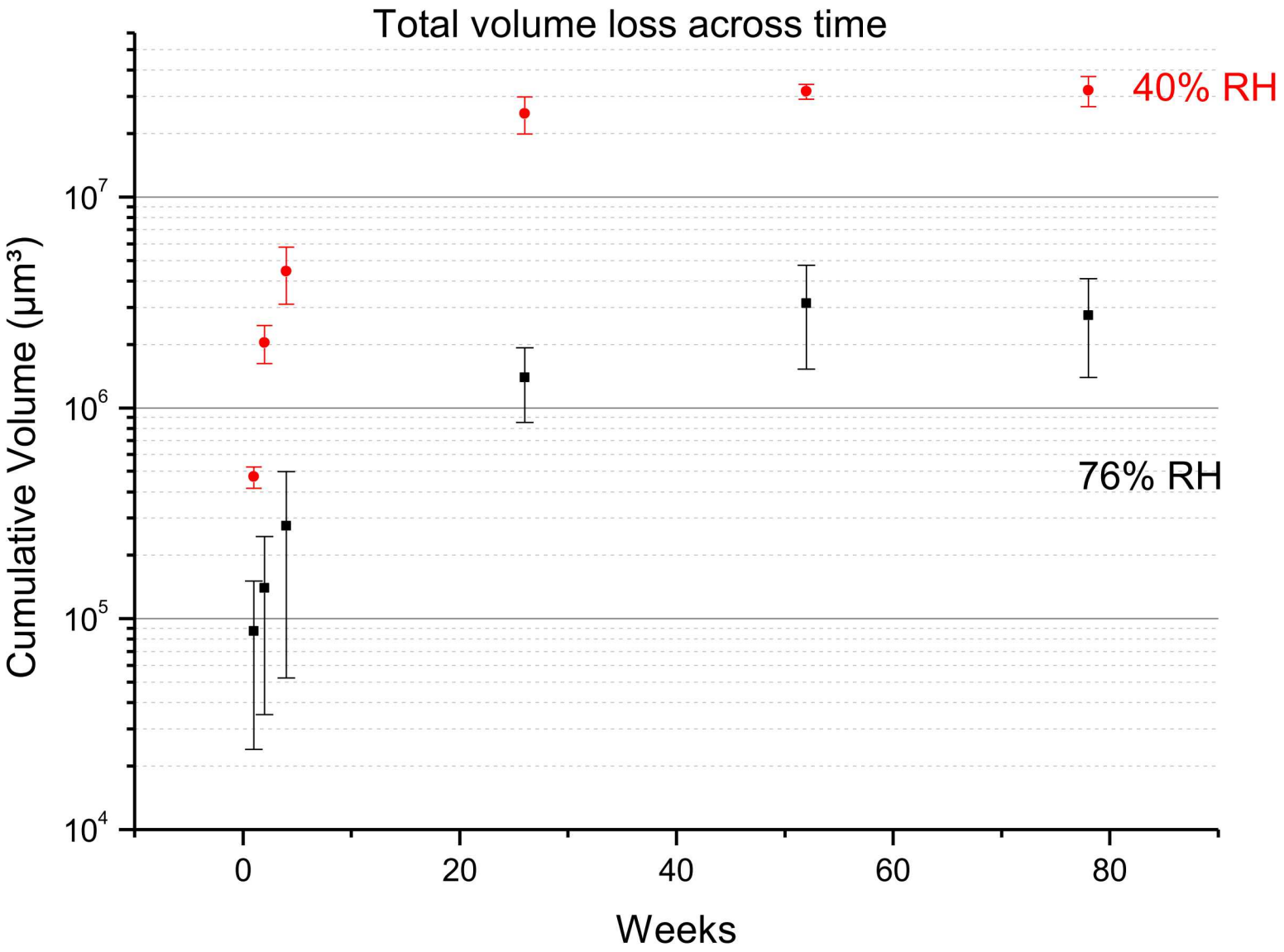
Total volume loss across time
40% RH
76% RH
Cumulative Volume (µm³)
10^7
10^6
10^5
10^4
0
20
40
60
80
Weeks

Surface coverage affects cathode availability
Cathodic resource competition at high RH

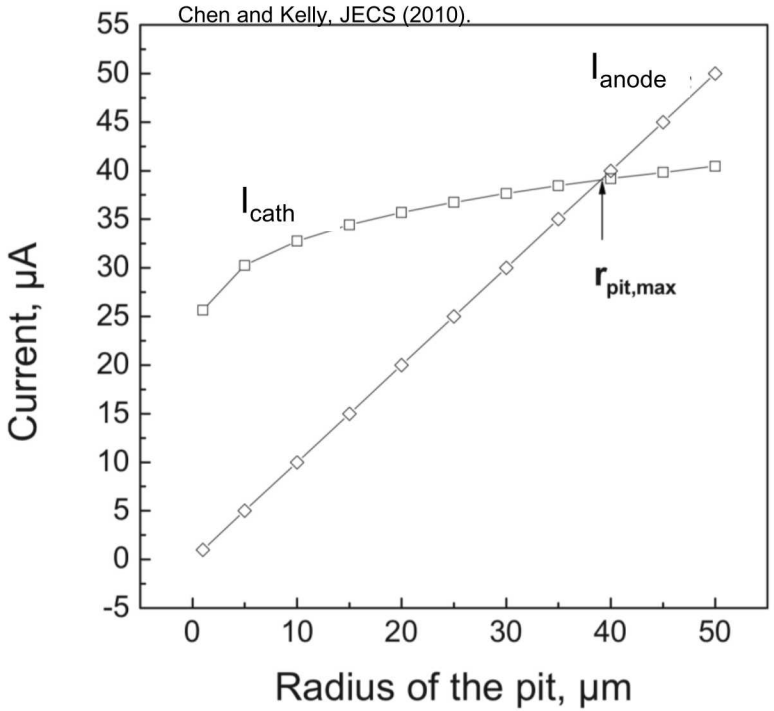

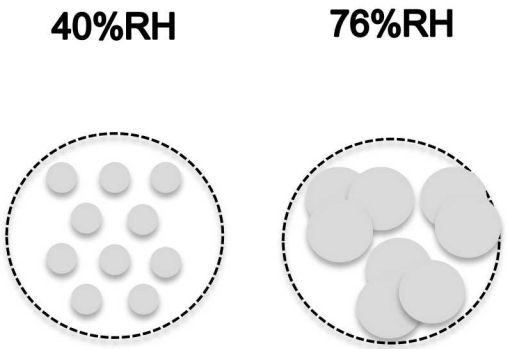

More surface coverage leads to cathodic resource limitation at high RH

Clustering results from cathodic current competition

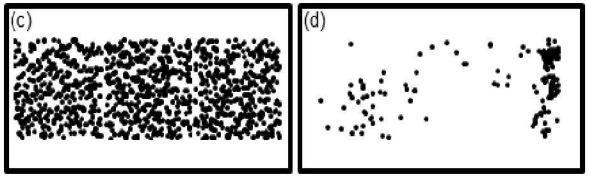

Discrete cathodes support growth of multiple pits that initiate at 40% RH

Possibility of SCC via HEAC at low RH?

Stress concentration

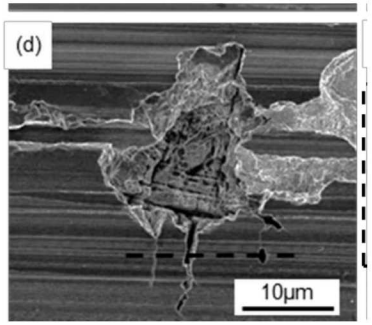

Weirich et al. JECS (2019).

HER ↑ near E_{rp}

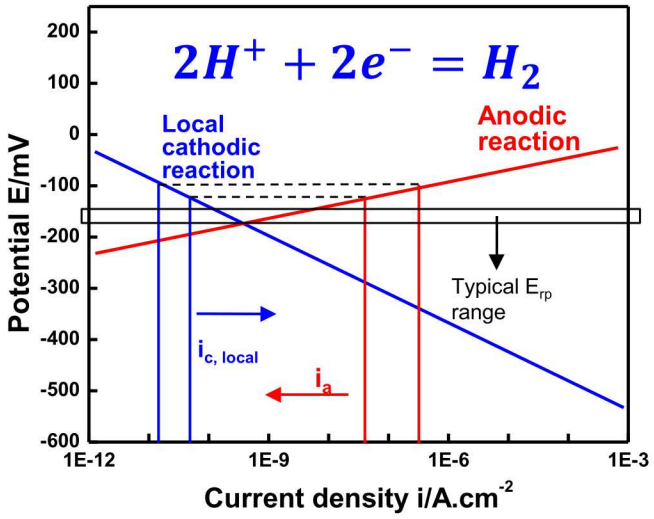

Srinivasan and Kelly, JECS (2016).

Sufficient residual stress

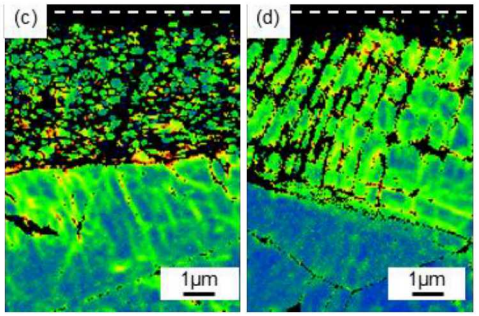

Weirich et al. JECS (2019).

Strain-induced martensite at near-surface layers?

Determining SCC risk of susceptible morphology

- Atmospheric exposure of salt applied on specimen gage length with induced artificial pit
- Loading sequence – constant (6h), intermediate cyclic (20 min, R = 0,7, f = 0.01, 0.1, 1 Hz)
- No Failure or visible crack after 44 days – sample pulled to failure

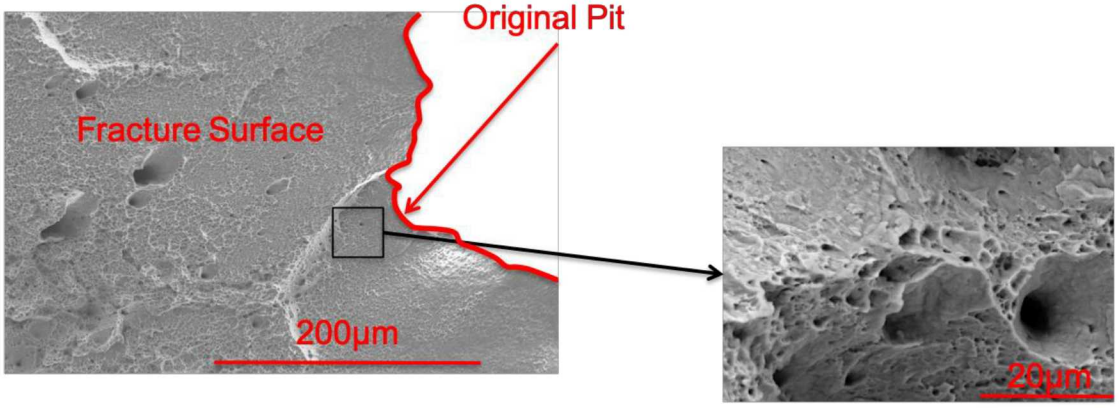

Smooth artificial pits
Insufficiently high load?
No wicking of electrolyte into initiator?

A change in pit density and pit distribution observed between the two humidity values

- Higher pit densities observed at 40%RH.
- Uniformity of pitting across the surface also observed on the 40%RH surface.

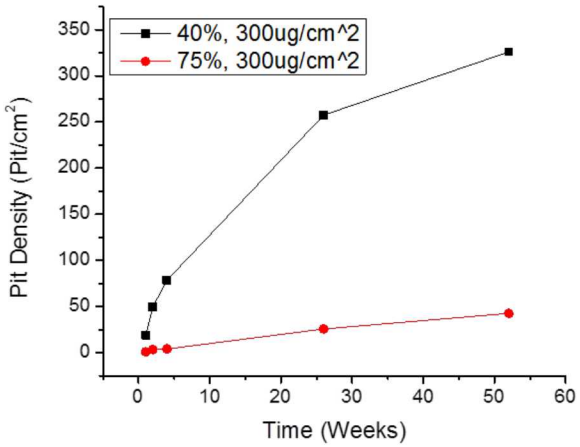

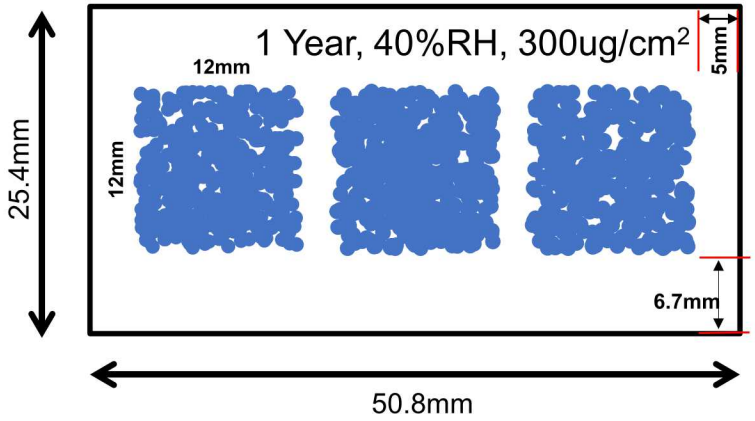

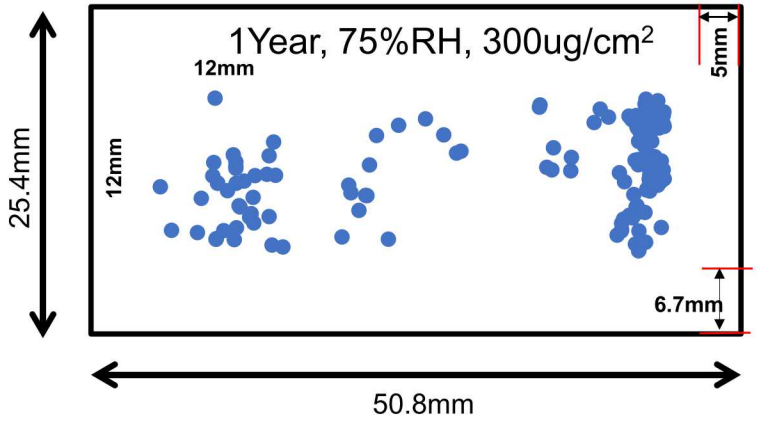

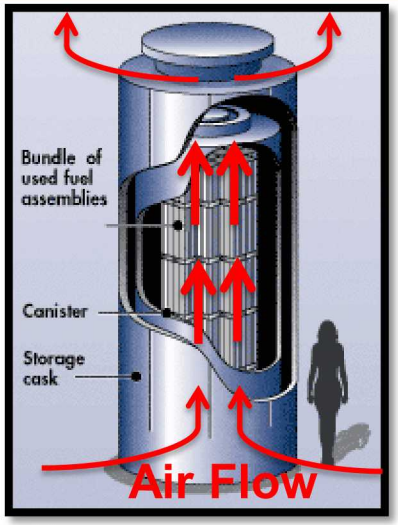

Source: www.nrc.gov